Deep inelastic $e^{\pm}p$ scattering at the highest Q^2

A.I. van Sighem
NIKHEF, P.O. Box 41882, 1009 DB Amsterdam, The Netherlands
Email: A.vanSighem@nikhef.nl

Abstract

¿From 1994 to 1999 each of the HERA experiments ZEUS and H1 collected about 40 pb^{-1} of e^+p and about 5 pb^{-1} of e^-p deep inelastic scattering data. These data allow the extraction of charged current and neutral current scattering cross sections in the high Q^2 region, up to 30000 GeV^2. Measurements of these cross sections by both experiments are presented and are compared to Standard Model predictions. The data provide evidence for Z boson exchange in the neutral current channel. ¿From the charged current measurements the mass of the space-like W boson can be extracted complementing the measurements of the mass of the time-like W boson from hadron-hadron and e^+e^- colliders.

1 Introduction

The internal structure of the proton can be probed by scattering pointlike particles like electrons or neutrinos off protons, a process known as deep inelastic scattering (DIS). In figure 1 a schematic diagram of this process is shown. An incoming positron with four-momentum k and an incoming proton with four-momentum P interact via the exchange of a gauge boson. This gauge boson couples to one of the (anti)quarks in the proton. This struck (anti)quark hadronises into the so-called current jet. The other constituents of the proton that do not take part in the hard interaction also hadronise and form the proton remnant. Two types of DIS can be distinguished: neutral current DIS where the exchanged boson is a photon or a Z particle, and charged current DIS which proceeds via W boson exchange.

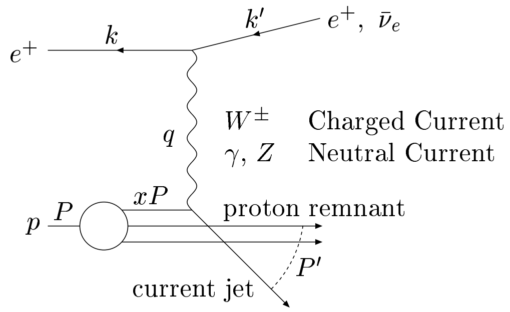

Figure 1: A schematic view of a deep inelastic scattering event.

The scale of the interaction, Q^2, is given by the square of the four-momentum q of the gauge boson:

$$Q^2 = -q^2 = -(k - k')^2 = -(P' - P)^2 \tag{1}$$

where k' is the four-momentum of the final state lepton and P' is the four-momentum of the hadronic final state. The second, independent variable that is often used to characterise a DIS event is Bjorken-x defined as

$$x = \frac{Q^2}{2P \cdot q} \tag{2}$$

In the "infinite momentum" frame of the proton x can be identified with the fraction of the momentum of the proton carried by the struck quark. In the proton rest frame the variable y which is defined as

$$y = \frac{P \cdot q}{P \cdot k} \tag{3}$$

is equal to the fraction of the energy of the positron that is transferred to the proton. The three kinematic variables x, y and Q^2 are related as

$$Q^2 = s\,x\,y \tag{4}$$

where the square of the centre-of-mass energy $\sqrt{s}$ is given as $s = (P+k)^2$.

The HERA ep collider offers the possibility to study DIS via electron-proton and positron-proton collisions at high centre-of-mass energies. First measurements of charged and neutral current DIS cross sections at values of Q^2 exceeding $\sim$ 200 GeV^2 have previously been published by the H1 and ZEUS collaborations [1, 2]. These analyses were based on e^-p and e^+p samples of approximately 1 pb^{-1} and 3 pb^{-1}, respectively. This paper presents results on charged and neutral current cross section measurements and comparisons with the Standard Model using the full amount of data collected in the period from 1994 to the beginning of 1999. In the years 1994 to 1997 HERA collided 820 GeV protons with 27.5 GeV positrons, yielding a centre-of-mass energy of 300 GeV. In 1998 and the first part of 1999 electrons were collided instead of positrons at the same energy, while the proton energy was raised to 920 GeV which resulted in a centre-of-mass energy of 318 GeV. The total integrated luminosities for the positron running equal 47 pb^{-1} for ZEUS and 37 pb^{-1} for H1 while the electron data amount to 6 pb^{-1} and 5.3 pb^{-1}, respectively. A description of both experiments can be found in [3].

2 Standard Model cross sections

The Standard Model prediction for the neutral current cross section $e^{\pm}p \rightarrow e^{\pm}X$ where X denotes the hadronic final state, is given by

$$\frac{d\sigma^{NC}(e^{\pm}p)}{dxdQ^2} = \frac{2\pi\alpha_{em}^2}{x}\frac{1}{Q^4} \times \left[Y_+F_2^{NC} - y^2F_L^{NC} \pm Y_-xF_3^{NC}\right] \tag{5}$$

where

$$\begin{aligned}
Y_{\pm} &= 1 \pm (1-y)^2 && (6)\\
F_2^{NC} &= \sum_f A_f(Q^2)\left[xq_f(x,Q^2) + x\bar{q}_f(x,Q^2)\right] && (7)\\
F_3^{NC} &= \sum_f B_f(Q^2)\left[xq_f(x,Q^2) - x\bar{q}_f(x,Q^2)\right] && (8)\\
A_f(Q^2) &= e_f^2 + 2e_ee_fv_ev_fP_Z + (v_e^2+a_e^2)(v_f^2+a_f^2)P_Z^2 && (9)\\
B_f(Q^2) &= 2e_ee_fa_ea_fP_Z + 4v_ev_fa_ea_fP_Z^2 && (10)
\end{aligned}$$

Here the label f denotes the quark flavour and e the incoming lepton with vector and axial vector couplings v_i and a_i. The Z propagator enters via $P_Z = Q^2/(Q^2+M_Z^2)$. In the quark-parton model the longitudinal structure function F_L vanishes. If only photon exchange is taken into account the parity violating term xF_3 is zero and $A_f = e_f^2$, the charge squared of quark flavour f.

The charged current cross section $e^{\pm}p \rightarrow \bar{\nu}_e(\nu_e)X$ is given as

$$\frac{d\sigma^{CC}(e^{\pm}p)}{dxdQ^2} = \frac{\pi\alpha_{em}^2}{4\sin^4\theta_w\, x}\frac{1}{(Q^2+M_W^2)^2} \times \begin{cases} \sum_i \left[x\bar{u}_i(x,Q^2) + (1-y)^2xd_i(x,Q^2)\right] & \text{for } e^+p \\ \sum_i \left[xu_i(x,Q^2) + (1-y)^2x\bar{d}_i(x,Q^2)\right] & \text{for } e^-p \end{cases} \tag{11}$$

with θ_w the Weinberg angle. The sum now runs over quark generations i. The electron and positron couple to different combinations of up- and down-type quarks and antiquarks due to the different charge of the exchanged W particle. Note that at low Q^2 the charged current cross section is suppressed by a factor $\mathcal{O}(M_W^4)$ compared to the neutral current cross section, while at high Q^2 the neutral and charged current cross sections become of the same order of magnitude.

At high Q^2 and high x the neutral current cross section is dominated by the u quark distribution as this distribution is about an order of magnitude larger than the d quark distribution and $e_u^2 = 4e_d^2$. The

e^+p charged current cross section is dominated by the d quark distribution since $d(x,Q^2) \gg \bar{u}(x,Q^2)$. On the other hand, the u quark distribution is dominating the e^-p charged current cross section. This yields a ratio of about an order of magnitude between the e^+p and e^-p charged current cross sections at high Q^2 and high x.

Finally, the reduced charged current cross section $\tilde{\sigma}^{CC}(e^\pm p)$ is defined as

$$\tilde{\sigma}^{CC}(e^\pm p) = \left[\frac{G_F^2}{2\pi x} \left(\frac{M_W^2}{M_W^2 + Q^2} \right)^2 \right]^{-1} \frac{d\sigma^{CC}(e^\pm p)}{dx\, dQ^2} \tag{12}$$

where the relation $G_F^2 M_W^4 / 2\pi = \pi\alpha_{em}^2 / 4 \sin^4\theta_w$ is used. The reduced neutral current cross section $\tilde{\sigma}^{NC}(e^\pm p)$ is defined analogously:

$$\tilde{\sigma}^{NC}(e^\pm p) = F_2^{NC} - \frac{y^2}{Y_+} F_L^{NC} \pm \frac{Y_-}{Y_+} x F_3^{NC} \tag{13}$$

3 Neutral current scattering results

A sample of neutral current DIS events is obtained by selecting events with a positron or electron in the final state. In addition the quantity $\delta = \sum_i E_i(1 - \cos\theta_i)$ should approximately be equal to twice the positron beam energy, $2E_e = 55$ GeV. Here the sum runs over all individual energy deposits E_i in the calorimeter with polar angle θ_i. Events are selected with an overall efficiency around 80% for both experiments. The overall remaining background is estimated to be less than 1%.

Figures 2a and 2b show the ZEUS measurement of the differential cross section $d\sigma/dQ^2$ and the ratio of this cross section to the Standard Model prediction for neutral current e^+p scattering. Between 400 GeV^2 and 20000 GeV^2 the cross section falls over six orders of magnitude. The Standard Model prediction evaluated using the CTEQ4D parton density functions (PDFs) [4] gives a very good description of the measured cross section. The uncertainty on this prediction due to imperfect knowledge of the PDFs is represented by a shaded band.

The H1 results on the reduced cross section $\tilde{\sigma}^{NC}(e^+p)$ are shown in figure 2c. For $Q^2 < 1000$ GeV^2 the error on the cross section is dominated by the systematic uncertainties, while at higher Q^2 the dominant error is statistical. The cross section rises steeply with decreasing x reflecting the increase in the sea quark and gluon densities at low x. The data are very well described by a NLO QCD fit, extrapolated to high Q^2, that has been performed on low Q^2 (< 120 GeV^2) measurements of F_2^p and F_2^d [5].

The data provide direct evidence for the presence of Z exchange in the space-like region explored by deep inelastic scattering. This is illustrated in figures 3a and 3b, which compare the measured cross sections $d\sigma/dQ^2$ and $d\sigma/dx$ with the Standard Model predictions, varying the mass of Z in the propagator to values of $M_Z = 40$ GeV, 91 GeV and infinity. Figure 3a shows the ratio of the measured cross section $d\sigma/dQ^2$ to the prediction of the Standard Model and figure 3b presents $d\sigma/dx$ as a function of x for $Q^2 > 10000$ GeV^2. The prediction with an infinite Z mass (figure 3b), i.e. no contribution of Z to the cross section, and that with a mass of 40 GeV (figure 3a) do not yield a description of the data as good as the prediction with nominal Z mass.

Preliminary measurements by H1 of $d\sigma/dQ^2$ for e^-p scattering are shown in figure 3c. The lines show the Standard Model expectations evaluated with the MRST set of parton densities [6]. At high Q^2 the e^-p cross section is larger than the e^+p cross section, reflecting the different contribution of the γZ interference term to both cross sections.

4 Charged current scattering results

Charged current events are selected by requiring that the invisible (anti)neutrino induces a substantial missing transverse momentum in the event. The overall background that remains after all selection cuts is less than 1%. In the lowest Q^2 region, however, the background can be as large as 10%. This is mainly due to photoproduction as this process can yield events with a topology similar to that of charged current events.

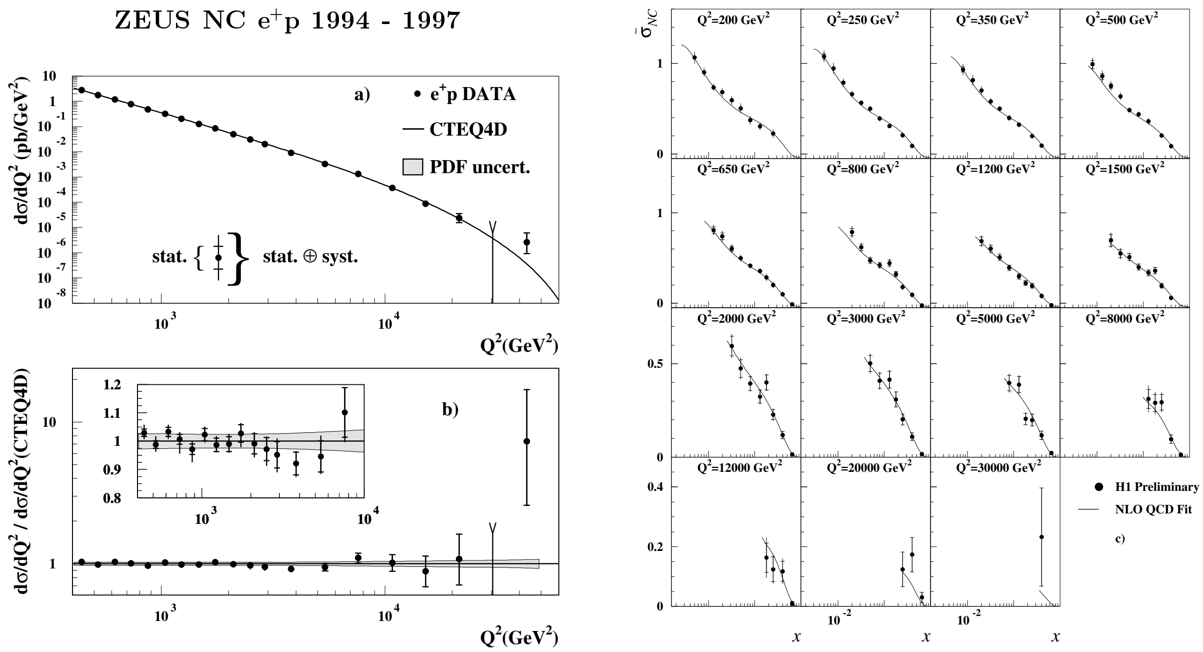

Figure 2: (a) Neutral current e^+p cross section $d\sigma/dQ^2$ measured by ZEUS and (b) the ratio of this cross section to the Standard Model prediction evaluated using the CTEQ4D PDFs. The shaded band shows the PDF uncertainty on the Standard Model prediction. (c) Reduced neutral current cross section $\tilde{\sigma}^{NC}(e^+p)$ measured by H1 as a function of x in bins of Q^2. The inner error bars (delimited by horizontal lines) show the statistical errors, the outer ones the statistical and systematic uncertainties added in quadrature.

In figure 3c the H1 measurements of the single differential cross sections $d\sigma/dQ^2$ are displayed for both electron and positron scattering. The plot shows that the e^-p cross section is twice as large as the e^+p cross section at low Q^2 and an order of magnitude larger at high Q^2 as expected from equation 11. The lines represent the Standard Model prediction as evaluated with the MRST set of parton density functions. Over the whole range in Q^2 the measured cross section is well described by the Standard Model prediction.

In figure 4a the reduced cross sections $\tilde{\sigma}^{CC}(e^+p)$ measured by ZEUS are displayed as a function of x in bins of Q^2. The lines show the prediction of the Standard Model evaluated using the CTEQ4D parton momentum distributions and the prediction of the ZEUS QCD fit [7]. This fit has been performed using data from fixed target experiments and previous NC DIS measurements at HERA in the region $Q^2 < 5000$ GeV^2. In leading order QCD the reduced cross section depends on the quark distribution functions as

$$\tilde{\sigma}^{CC}(e^+p) = x\left[\bar{u} + \bar{c} + (1-y)^2(d+s)\right] \tag{14}$$

As a result, for fixed Q^2, $\tilde{\sigma}^{CC}(e^+p)$ at low x, i.e. high y, is mainly sensitive to the antiquark combination $\bar{u} + \bar{c}$ while at high x, i.e. low y, it is dominated by the quark combination $d + s$. In the figure the contributions of both $x(\bar{u}+\bar{c})$ and $(1-y)^2\, x(d+s)$ to the cross section are shown as a function of x. These combinations of parton densities are evaluated with the leading order QCD CTEQ4L parametrisation [4]. The data clearly demonstrate the presence of both components. Both the quark and the antiquark contributions are required to obtain a good description of the data.

Figures 4b and 4c show the measured cross section $d\sigma/dx$ as a function of x for $Q^2 > 200$ GeV^2 and the ratio of this cross section to the Standard Model prediction. At high x the cross section shows a tendency to be above the CTEQ4D prediction. However, no stronger conclusions can be drawn from this observation since the uncertainty on the predicted cross section is rapidly growing beyond $x = 0.4$ as indicated by the shaded band. The ZEUS NLO QCD fit describes the data very well and follows the trends of the data at high x better than the CTEQ4D prediction. This is because the fit yields a larger

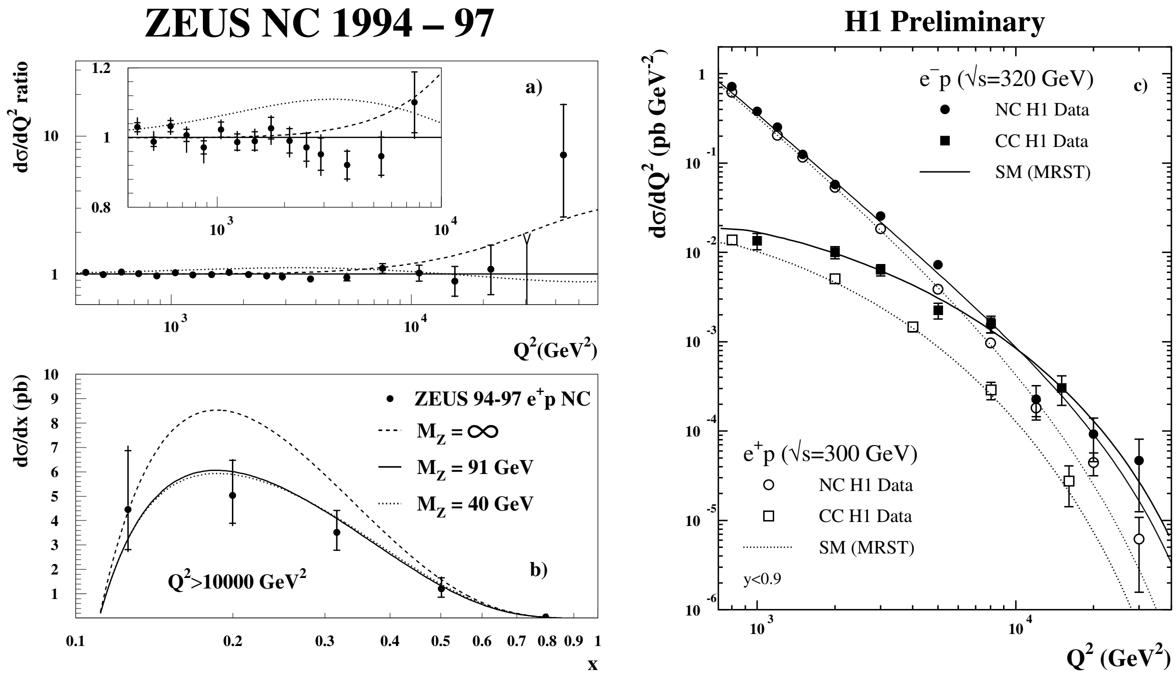

Figure 3: (a) Ratio of the cross section $d\sigma/dQ^2$ to the Standard Model prediction and (b) $d\sigma/dx$ for $Q^2 > 10000$ GeV^2. The lines in both figures show the predictions with varying Z mass. (c) Neutral and charged current cross sections $d\sigma/dQ^2$ for e^+p and e^-p scattering.

d/u quark ratio at high x compared to CTEQ4D. The possibility of a larger d/u ratio than previously assumed has recently been investigated, see for example [8, 9]. An artificial modification of the d density with a term $\delta(d/u) = 0.1\,x(x+1)$, as suggested in [9], yields a $d\sigma/dx$ very close to the QCD fit as shown in figure 4c by the dotted line labeled as Yang-Bodek. The MRST set of parton momentum distributions, which includes the E866 measurement [10] of $x(\bar{d}-\bar{u})$ that (partially) drives the d/u ratio at high x, also predicts a larger cross section than CTEQ4D in this region.

The cross section $d\sigma/dQ^2$ is determined by the Fermi constant G_F, a term containing the dependences on the parton density functions and a propagator term $M_W^2/(M_W^2+Q^2)$. A χ^2 fit to the measured cross section treating G_F and M_W as free parameters yields

$$M_W = 80.9^{+4.9}_{-4.6}(\text{stat})^{+5.0}_{-4.3}(\text{syst})^{+1.3}_{-1.2}(\text{PDF})\ \text{GeV}\quad (\text{ZEUS}) \tag{15}$$

$$M_W = 81.2 \pm 3.3(\text{stat}) \pm 4.3(\text{syst})\ \text{GeV}\quad (\text{H1}) \tag{16}$$

The PDF error quoted by ZEUS is obtained by re-evaluating the W mass while varying the parton density functions within the uncertainties given by the ZEUS NLO QCD fit. These values of M_W agree with the current world average of $M_W = 80.41 \pm 0.10$ GeV [11].

Another fit to $d\sigma/dQ^2$ has been performed in which G_F is fixed to the PDG value 1.16639×10^{-5} GeV^{-2} [11]. This yields the result

$$M_W = 80.4^{+2.7}_{-2.6}(\text{stat})^{+2.0}_{-2.0}(\text{syst})^{+3.3}_{-3.0}(\text{PDF})\ \text{GeV}\quad (\text{ZEUS}) \tag{17}$$

The use of the G_F constraint significantly reduces the uncertainty on the determination of M_W as compared to the previous fit. These two fits constitute an important consistency check of the Standard Model as they measure the mass of the space-like W boson rather than that of the time-like W that is measured at hadron-hadron and e^+e^- colliders.

A third fit is performed by ZEUS by evaluating the χ^2 function of the ZEUS data along the Standard Model constraint

$$G_F = \frac{\pi\alpha_{em}}{\sqrt{2}} \frac{M_Z^2}{M_W^2(M_Z^2 - M_W^2)} \frac{1}{1-\Delta r(M_W)} \tag{18}$$

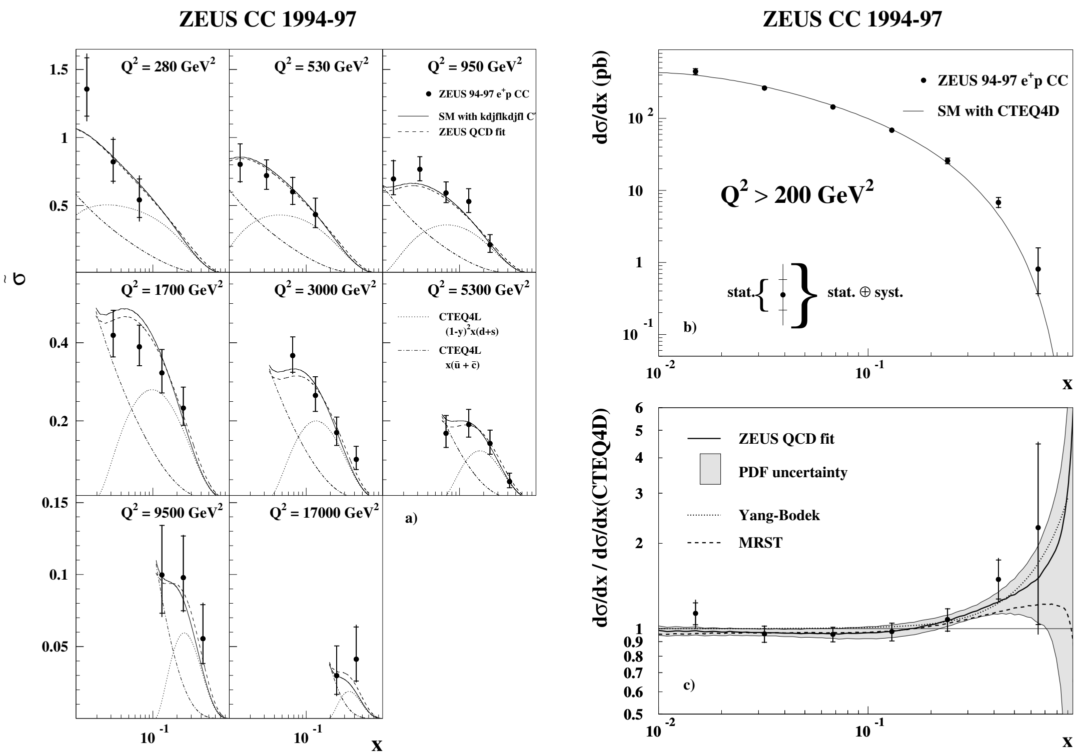

Figure 4: (a) Charged current reduced cross section $\tilde{\sigma}^{CC}(e^+p)$ as a function of x in bins of Q^2. (b) Cross section $d\sigma/dx$ for $Q^2 > 200$ GeV^2 and (c) the ratio of $d\sigma/dx$ to the Standard Model expectation.

The factor Δr contains the radiative corrections to the lowest order expression for G_F and is a function of α_{em} and the masses of the fundamental bosons and fermions. Taking $m_t = 175$ GeV and $M_H = 100$ GeV the fit yields a W mass

$$M_W = 80.50^{+0.24}_{-0.25}(\text{stat})^{+0.13}_{-0.16}(\text{syst})^{+0.30}_{-0.31}(\text{PDF})^{+0.05}_{-0.06}(\Delta m_t, \Delta M_H)\ \text{GeV}\quad (\text{ZEUS}) \tag{19}$$

where the error labeled as $(\Delta m_t, \Delta M_H)$ is obtained by re-evaluating M_W with the top quark mass m_t in the range $170 < m_t < 180$ GeV and the Higgs mass M_H in the range $100 < M_H < 220$ GeV. The total error on M_W is an order of magnitude smaller than in the previous two fits due to the strong dependence of M_W on G_F implied by the Standard Model constraint, equation 18. It should be noted, however, that this latter fit is merely a consistency check of the Standard Model and not an independent measurement of M_W since it assumes the validity of the Standard Model.

References

[1] H1 collaboration, Phys. Lett. B324 (1994) 241.
H1 collaboration, Z. Phys. C67 (1995) 565.
H1 collaboration, Phys. Lett. B379 (1996) 319.

[2] ZEUS collaboration, Phys. Rev. Lett. 75 (1995) 1006.
ZEUS collaboration, Z. Phys. C72 (1996) 47.

[3] ZEUS collaboration, The ZEUS detector, Status Report 1993, DESY 1993.
H1 collaboration, Nucl. Instrum. Methods 386 (1997) 310 and 348.

[4] H.L. Lai et al., Phys. Rev. D55 (1997) 1280.

[5] H1 collaboration, ICHEP 98–Vancouver, 98–533 (1998).

[6] A.D. Martin, R.G. Roberts, W.J. Stirling and R.S. Thorne, Eur. Phys. J. C4 (1998) 463.
A.D. Martin, R.G. Roberts, W.J. Stirling and R.S. Thorne, hep-ph/9907231.

[7] ZEUS collaboration, Z. Phys. C72 (1996) 399.
M. Botje, NIKHEF-99–011 (1999).
[8] W. Melnitchouk and A.W. Thomas, Phys. Lett. B377 (1996) 11.
W. Melnitchouk and J.C. Peng, Phys. Lett. B400 (1997) 220.
[9] U.K. Yang and A. Bodek, Phys. Rev. Lett. 82 (1999) 2467.
[10] E866 collaboration, Phys. Rev. Lett. 80 (1998) 3715.
[11] Particle Data Group, Eur. Phys. J. C3 (1998) 1.